JOURNAL OF MATERIALS SCIENCE 28 (1993) 1351–1359

Influence of compositional variables and testing temperature on the wear of hydrogenated nitrile rubber

P. THAVAMANI, A. K. BHOWMICK
Rubber Technology Centre, Indian Institute of Technology, Kharagpur 721302, India

The influence of the nature and level of the curing system, the loading of carbon black and the resin content on the abrasion loss, V, dynamic coefficient of friction, μ, and frictional force, F, of hydrogenated nitrile rubber (HNBR) against silicone carbide abrader, is reported at different temperatures. V, μ, and F decrease with cross-link density. At equal cross-link density, these parameters are the same for both peroxide and sulphur-curing systems. Incorporation of resin decreases V, μ, and F progressively. V decreases, but μ and F increase with loading of carbon black at any particular testing temperature, and the opposite trend is observed with increasing temperature. Experimental results on natural rubber (NR) and styrene–butadiene rubber (SBR) are also compared with those of HNBR. The abrasion loss of HNBR is much lower than that of NR and SBR. The abraded surface of NR and SBR is tar-like and ridges are found at all temperatures. In the case of HNBR compounds no ridge, except plough marks in the direction of abrasion, is observed at 25 °C. However, at high temperature (>50 °C) the abrasion mechanism changes, and ridge formation takes place. The ridge spacing, R_s, reduces with carbon black loading and decreasing temperature. R_s is related to dynamic shear modulus, G', by $R_s = \text{const.}\ (1/G')^{1.55}$. V increases linearly with R_s. The abradability, A, is related to reciprocal of breaking energy, E_b, by $A = C/E_b$, where C is a constant having a value of the order of 10^{-12} m^3

1. Introduction

Wear of rubber is a complex phenomenon and depends on many factors such as the nature of the matting surfaces, composition and mechanical properties of vulcanizates, testing temperature, strain rates, etc. It is further complicated by mechanochemical and thermochemical degradation of vulcanizates. Various mechanisms have been proposed for rubber abrasion. Schallamach [1] reported pattern formation on the abraded surface of natural rubber (NR) using a needle as an abrader and related the pattern spacings to the modulus of the rubber. Champ *et al.* [2] studied the wear mechanism using a razor blade as an abrader, and proved that abrasion took place due to cumulative crack growth. According to Gent and Pulford, however, abrasive wear could not be solely determined by crack-growth properties, but other fracture processes might also be involved [3]; Pulford [4] subsequently reviewed the mechanism of rubber abrasion. Grosch [5] discussed the role of viscoelastic energy losses at different temperatures and velocities on friction and found a relation between abradability and reciprocal of breaking energy [6]. The friction of nitrile rubber vulcanizate against a glass cylinder was reported to be a function of viscoelastic properties [7].

Hydrogenated nitrile rubber (HNBR) finds an increasing number of applications as an ideal engineering material due to its good heat- and oil-resistance properties [8]. Recently, Medalia *et al.* [9] reported that HNBR tank track pads showed superior abrasion resistance in the field. Preliminary studies of wear of HNBR against rock under laboratory conditions reveal its excellent abrasion resistance [10]. The track pads, however, are damaged at high temperature and under severe stress–strain conditions in the field. In order to understand the wear mechanism, an experimental investigation has been carried out on the effect of compositional variables and testing temperature on the abrasion loss, V, dynamic coefficient of friction, μ, and frictional forces of HNBR. The nature and level of the curing system, the loading of carbon black and the resin content in the recipe have been varied. An attempt has been made to relate wear with dynamic mechanical properties. Experiments with natural rubber (NR) and styrene butadiene rubber (SBR) are also reported for comparison. The present study is important in understanding the wear of rubbers when viscoelastic energy losses are minimized by increasing the test temperature.

2. Experimental procedure

2.1. Materials

HNBR (ZETPOL 1020) and resin (ZSC 2295) were obtained from Nippon Zeon Co.Ltd, Japan. Carbon black (N110) was obtained from Philips Carbon Black

0022–2461

Ltd, India. The dicumyl peroxide "DI-CUP R" was obtained from Hercules Incorporated, USA. Other materials, such as zinc oxide, stearic acid, sulphur, etc., were chemically pure.

2.2. Abrasion specimen preparation

All the compounds given in Tables I and II were mixed in a laboratory mill as per the standard procedure. The rubber specimens for abrasion (20×20 mm^2) were prepared by moulding in an electrically heated hydraulic press at 160 °C to its optimum cure state (as determined from rheometry).

2.3. Wear apparatus and measurement of μ, *V* and *A*

A modified Du Pont Abrader, as shown in Fig. 1, was used to measure the abrasion loss, V, abradability, A, dynamic coefficient of friction, μ, and frictional work, W. Two rubber specimens were clamped on the lever arm and the end of the lever was attached to a load cell to measure the torque and hence the tangential force acting at the rubber–abrader interface. The abrader (silicone carbide abrasive paper having grain size of 325 mesh) was fixed on a disc and load was applied normal to the rubber specimen by hanging a weight using a string and a pulley. One end of the string was tied to the weight and the other end with a rod attached to the lever arm. The abrader and the rubber specimens were kept inside a chamber and its temperature was maintained within ± 2 °C variation by blowing hot air. The experiments were carried out at 25, 50, 75 and 100 °C for 10 min after conditioning the samples for 15 min. μ, V and A were calculated from the torque and weight loss [10].

TABLE I Formulae of compounds

Ingredients	Compound reference (p.h.r.)							
	D1	D2	D3	D4	D5	D6	D7	D8
ZETPOL 1020[a]	100	100	100	100	90	80	70	60
ZSC 2295[b]	–	–	–	–	10	20	30	40
Zinc oxide	2	2	2	5	2	2	2	2
Stearic acid	–	–	–	1	–	–	–	–
Sulphur	–	–	–	0.5	–	–	–	–
Carbon black N110	50	50	50	50	30	30	30	30
TMTD[c]	–	–	–	2	–	–	–	–
MBT[d]	–	–	–	0.5	–	–	–	
Di-cup R	4.5	3.0	1.5	–	3.0	3.0	3.0	3.0
Total	156.5	155.0	153.5	159.0	135.0	135.0	135.0	135.0

[a]Hydrogenated nitrile rubber with 44% acrylonitrile content and 25 g/100 g iodine number.
[b]Commercially available resin. It contains 15 p.h.r. ZnO and 20 p.h.r. methyl acrylic acid (MAA) in HNBR. (Private communication received from the manufacturer.)
[c]Tetramethyl thiuram disulphide.
[d]Mercapto benzothiazole.

TABLE II Formulae of compounds

Ingredients	Compound reference (phr)						
	D9	D10	D11	D12	D13	H4	H8
ZETPOL 1020	100	100	100	100	100	–	–
NR	–	–	–	–	–	100	–
SBR	–	–	–	–	–	–	100
Zinc oxide	2	2	2	2	2	5	5
Stearic acid	–	–	–	–	–	6	6
TMQ[a]	–	–	–	–	–	0.5	0.5
Pilflex 13[b]	–	–	–	–	–	3	3
Carbon black N110	–	10	20	30	40	50	50
Di-cup R	3	3	3	3	3	–	–
HBS[c]	–	–	–	–	–	0.8	0.8
Sulphur	–	–	–	–	–	2	2
PVI[d]	–	–	–	–	–	0.5	0.5
Total	105	115	125	135	145	167.8	167.8

[a]2,2,4-trimethyl-1,2-dihydroquinoline.
[b]*N*-(1,3-dimethylbutyl)-*N*′-phenyl-p-phenylene-diamine.
[c]*N*-cyclohexyl-2-benzothiazole sulphenamide.
[d]*N*-(cyclohexylthio) phthalimide.

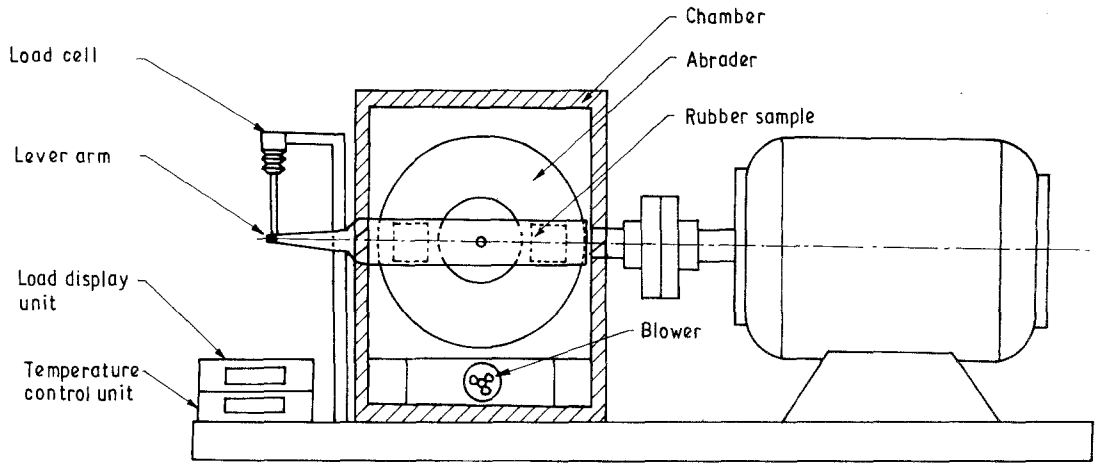

Figure 1 Schematic diagram of the abrader.

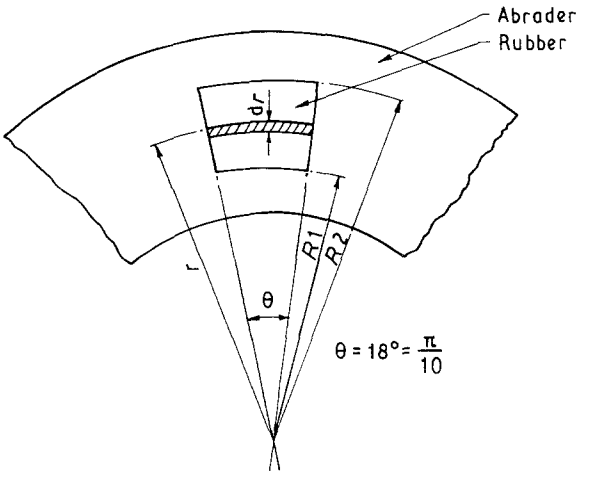

Figure 2 A segment of rubber–abrader contact surface.

From Fig. 2, the dynamic coefficient of friction, μ, may be written as

$$\mu = 3/2\ \tau/P\left(\frac{R_2^2 - R_1^2}{R_2^3 - R_1^3}\right) \quad (1)$$

where τ is the torque (Nm), and P the normal load (N).

$$\text{Frictional work, } W = \frac{\mu P d}{a}\ \text{Jm}^{-2} \quad (2)$$

where d is the circumferential length of the abrader track (m), and a the area of the specimen in contact with abrader (m^2)

$$A = V/W \quad (3)$$

where V is the abrasion loss ($m^3\ rev^{-1}$). The values reported here are the averages of three separate experiments.

2.4. Dynamic mechanical properties

Dynamic mechanical properties, i.e. storage shear modulus, G', and $\tan\delta$, were measured using a Polymer Laboratories PL-DMTA Unit in the shear mode of deformation with double strain amplitude of 64 μm at 10 Hz and 1 °C min^{-1} heating rate. The data acquired were analysed, using a COMPAQ computer. The frequency of deformation during abrasion was calculated from the number of grains per unit length and the rate of abrasion. The data acquired at 10 Hz were transformed to the frequency of deformation (1.5×10^4 Hz) involved during abrasion, using the Universal Williams–Landel–Ferry (WLF) rate–temperature shift factor, $\log a_T$ [11]

$$\log a_T = -17.4(T - T_g)/(51.6 + T - T_g) \quad (4)$$

where T_g is the glass transition temperature of the rubber.

2.5. Determination of tensile and tear strength and breaking energy, E_b

Tensile and tear strengths of all the compounds were determined using ZWICK UTM 1445 interfaced with a computer. The breaking energy was obtained from the area under the stress–strain curve, directly from the interfaced computer.

2.6. Volume fraction of rubber

The volume fraction of rubber, V_r, in ethyl acetate solvent was determined using the following relation [12]

$$V_r = \frac{(D - I_F S_W)/\rho_r}{[(D - I_F S_W)/\rho_r] + (A_o/\rho_s)} \quad (5)$$

where D is the unswollen weight of the sample, I_F the weight fraction of insoluble components, S_W the sample weight, ρ_r, ρ_s the density of rubber and solvent, respectively, and A_o the amount of solvent imbibed after suitable correction.

2.7. Studies of the fracture surface

The abraded surface was sputter coated with gold and examined under a scanning electron microscope (SEM) (model 2DV Cam Scan, UK). Scanning electron micrographs of the ridges were taken at higher

magnification (× 300 to × 500) to measure the ridge spacings. All the samples were tested within 48 h.

3. Results and discussion

3.1. Effect of cross-link density and curing system

Figs 3 and 4 show the effect of cross-link density and curing system on abrasion loss, V, dynamic coefficient of friction, μ, and frictional force, F, at different temperatures for the compounds D1, D2, D3 and D4. Wear increases with temperature for all compounds. The cross-link density of these systems follows the order D1 > D2 = D4 > D3 (Table III). The abrasion loss decreases with the increase in cross-link density. Sulphur-cured (D4) and peroxide-cured (D2) systems display almost similar volume loss. Although the C–S and S–S bonds in the sulphur-cured system are more susceptible to thermo-oxidative degradation and are reported to have better fatigue properties in natural rubber [13], the abrasion loss of D4 even at 100°C is comparable to that of peroxide-cured D2. This is due to the high thermal stability of HNBR [8]. The observed increase in abrasion loss with reduction in cross-link density and increase in test temperature is partly due to decrease in strength and breaking energy (Table III). There is approximately 50%–60% loss in tensile strength on raising the test temperature from 25°C to 100°C.

The dynamic coefficient of friction and frictional force also decrease with cross-link density and temperature (Fig. 4). D2 and D4 compounds show almost similar behaviour. The above observations could be explained as follows. The total frictional force generated at the sliding interface consists of two components, adhesional, F_A, and hysteresis, F_H [14].

$$F = F_A + F_H \tag{6}$$

F_A is attributed to the molecular bonding between the exposed surface atoms of rubber and abrader. Any sliding action causes these bonds to stretch, rupture and relax before new bonds are formed; F_A is predominant when the abrasion is against a smooth surface. F_H arises when the sharp asperities on the rough abrader move over the rubber surface. If F_A and F_H in Equation 6 are replaced by [14]

$$F_A = K_1 S(E'/P^r)\tan\delta \qquad (r < 1) \tag{7}$$

and

$$F_H = K_2(P/E')^n \tan\delta \qquad (n \geqq 1) \tag{8}$$

the total frictional force, F, becomes

$$F = [K_1 S(E'/P^r) + K_2(P/E')^n]\tan\delta \tag{9}$$

where P is the normal load, E' is the storage modulus and S is the effective shear strength of the sliding interface. As shown in Table III and reported earlier [15] hysteresis loss as measured by tan δ increases with decreasing cross-link density at any particular temperature, whereas the hysteresis decreases with temperature for all the compounds. Hence, μ and F decrease with temperature and cross-link density.

3.2. Effect of resin

The effect of resin on abrasion loss, and μ and F at different temperatures is shown in Figs 5 and 6, respectively. The abrasion loss at all temperatures decreases exponentially up to 30 p.h.r. resin. At 25°C, however, this change of volume loss with resin is not sharp. The incorporation of resin in HNBR increases the strength properties and improves its heat resistance (Table III). 30 p.h.r. resin is found to be optimum. Hence, the abrasion loss decreases exponentially up to 30 p.h.r. and reaches constant value above 30 p.h.r. Because the heat resistance is improved, the abrasion loss at high temperature decreases drastically with resin concentration.

μ and F also decrease with increasing resin concentration and temperature. The dynamic mechanical properties indicate that the hysteresis (tan δ) decreases with resin concentration and temperature. Because

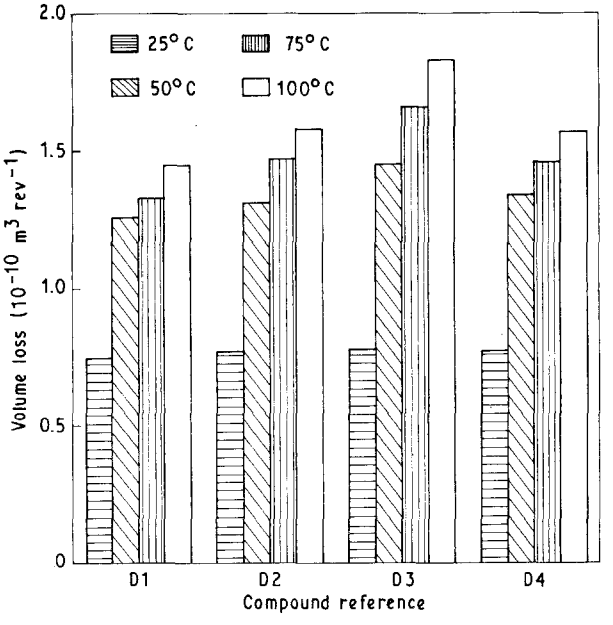

Figure 3 Variation of abrasion loss with cross-link density at different temperatures.

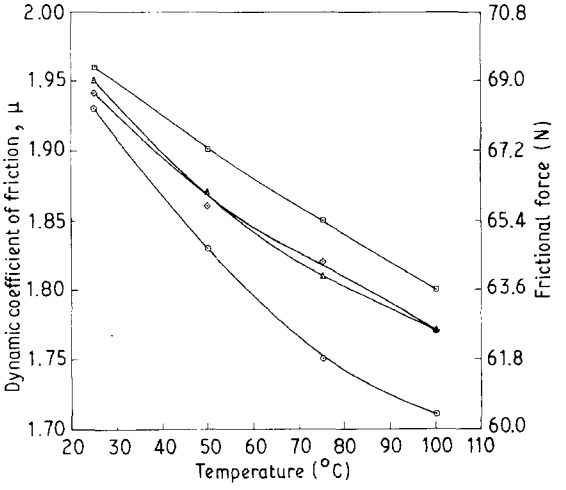

Figure 4 Variation of dynamic coefficient of friction, μ, and frictional force, F, with cross-link density at different temperatures. (○) D1, (△) D2, (□) D3, (◇) D4.

TABLE III Physical properties of compounds

Properties	Compound Reference							
	D1	D2	D3	D4	D5	D6	D7	D8
Optimum cure time at 160°C (min)	16	16	16	8	16	15	15	15
Specific gravity	1.15	1.15	1.15	1.17	1.13	1.15	1.18	1.18
Hardness (Shore A)	79	77	72	77	70	75	80	85
Tensile strength (MPa):								
25°C	36	32	30	31	35	37	39	39
50°C	32	29	24	32	29	32	34	35
75°C	22	20	18	22	23	27	29	30
100°C	17	14	12	16	15	16	18	20
After ageing at 120°C/70 h	33	29	27	29	33	36	38	38
300% modulus (MPa)	34.2	26.1	14.5	19.5	20.5	27.3	30.3	36.2
Elongation to break (%)	320	400	600	500	450	400	350	320
Tear strength (N cm^{-1})	920	855	800	830	960	980	1010	1090
Volume fraction of rubber, V_r	0.456	0.419	0.338	0.416	0.474	0.489	0.497	0.511
Breaking energy (kJ m^{-2}):								
25°C	28.7	27.8	23.8	27.6	28.5	29.1	29.5	29.8
50°C	23.5	22.7	19.1	23.0	23.8	25.9	26.2	26.6
75°C	16.6	15.8	13.0	16.0	15.8	17.4	18.7	18.8
100°	11.8	10.3	7.5	10.8	11.7	12.3	14.6	14.9
Tan δ:								
50°C	0.157	0.164	0.167	0.163	0.148	0.138	0.123	0.118
75°C	0.152	0.162	0.163	0.161	0.149	0.137	0.121	0.110
100°C	0.145	0.155	0.158	0.154	0.145	0.134	0.118	0.108

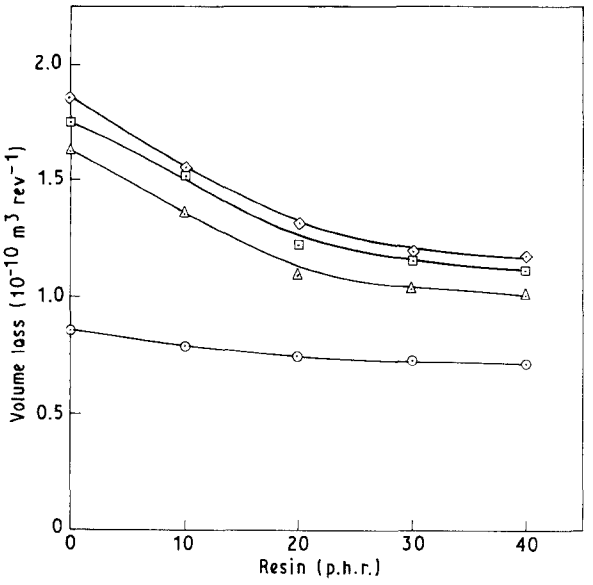

Figure 5 Variation of abrasion loss with resin loading at different temperatures. (○) 25°C, (△) 50°C, (□) 75°C, (◇) 100°C.

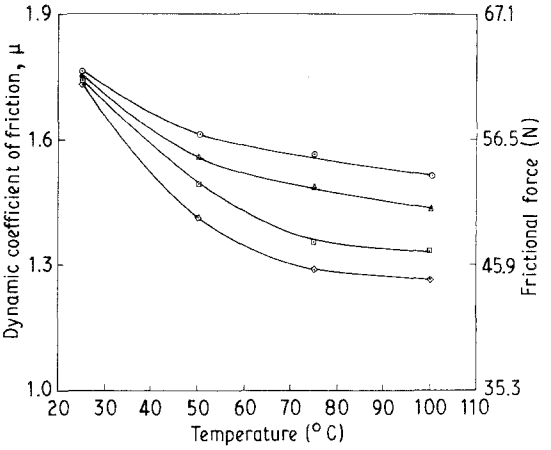

Figure 6 Variation of μ and F with resin loading at different temperatures. (○) D5, (△) D6, (□) D7, (◇) D8.

F decreases with resin concentration, the frictional energy available for abrasion is less. This, in addition to the improvement in heat resistance, accounts for the reduced loss with resin concentration.

3.3. Effect of carbon black

Figs 7 and 8 show the variation of volume loss, V, μ and F, at different temperatures with loading of carbon black. As expected the abrasion loss decreases with loading due to reinforcement of the rubber matrix (Table IV). μ and F increase with loading at all the temperatures. The incorporation of carbon black into rubber raises the hysteresis hydrodynamically as

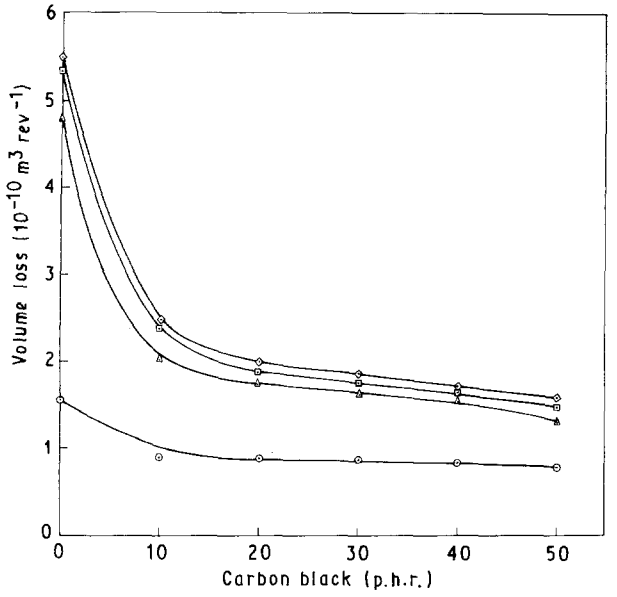

Figure 7 Variation of abrasion loss with carbon black loading at different temperatures. (o) 25°C, (△) 50°C, (□) 75°C, (◇) 100°C.

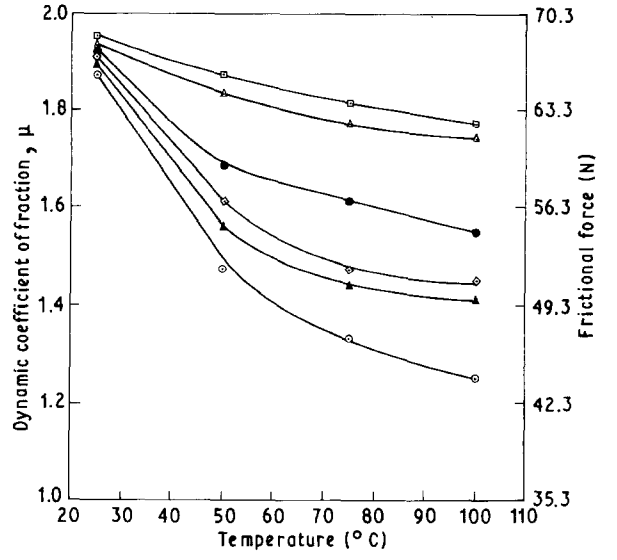

Figure 8 Variation of μ and F with carbon black loading at different temperatures. (o) D9, (▲) D10, (◇) D11, (●) D12, (△) D13, (□) D2.

well as through a network mechanism and strain amplification. Payne and Whittaker [16] reported that the carbon black network formation produced a significant increase in E' and E'' at low strain amplitude, the latter being affected to a greater degree and hence increasing tan δ. This accounts for the increase of μ and F with loading of carbon black (Equation 9). Staklis [17] reported similar observation for butyl rubber up to 55–65 p.h.r. SAF black loading. With rise of temperature, the hydrodynamic effect and the degree of strain amplification are reduced [18] and hence μ and F decrease with temperature. Grosch [6] reported that above the rubber–glass transition region, μ and F decrease with temperature. Despite the decreasing frictional force, the volume loss increases with temperature. This may be due to the fact that the critical tearing energy and the fatigue resistance are reduced at high temperature [19].

TABLE IV Physical properties of compounds

Properties	Compound reference				
	D9	D10	D11	D12	D13
Optimum cure time at 160°C (min)	16	16	16	16	16
Specific gravity	0.99	1.04	1.08	1.12	1.14
Hardness (Shore A)	51	56	62	65	71
Tensile strength (MPa):					
25°C	11	25	29	30	32
50°C	8	17	19	26	28
75°C	6	11	16	21	23
100°C	4	6	8	11	15
300% modulus (MPa)	2.5	5.3	13.5	21.2	25.0
Elongation to break (%)	600	500	450	400	400
Tear strength (N cm^{-1})	350	430	480	710	770
Volume fraction of rubber, V_r	0.425	0.436	0.441	0.443	0.447
Breaking energy (kJ m^{-2}):					
25°C	9.2	16.9	25.9	27.2	27.4
50°C	3.5	10.1	17.1	20.1	21.3
75°C	1.5	7.6	9.0	12.0	14.8
100°C	0.6	0.8	2.5	3.8	9.8
Tan δ:					
50°C	0.128	0.138	0.147	0.158	0.163
75°C	0.123	0.131	0.143	0.157	0.159
100°C	0.109	0.119	0.129	0.147	0.152

3.4. Nature of the polymer

The abrasion loss of NR, SBR and HNBR compounds, containing 50 p.h.r. SAF carbon black at different temperatures are shown in Fig. 9. The abrasion loss for all the rubbers increases with temperature in the order SBR > NR > HNBR. In the case of HNBR, the abrasion loss increases sharply from 25–50°C due to the change in the nature of the rubber surface in contact with the abrader, as explained later. The subsequent increase is slow. In NR and SBR compounds the abrasion loss increases with temperature in a similar manner. The abraded surface of HNBR at all the temperatures is dry and the debris are particulate, whereas the abraded surface of NR and SBR is tacky, producing debris in the form of tar-like and gummy residue due to the thermochemical degradation. The abrasion loss of NR and SBR levels off above 100°C due to the formation of an oily layer at the interface which protects the rubbers from further removal by abrader. Similar observations of oily layer formation were reported earlier [3]. At all the temperatures the abrasion loss of NR is less than that of SBR. μ and F follow the same trend as abrasion loss and could explain the variation of abrasion loss with the nature of the rubber and temperature.

3.5. Relation between abradability, A and breaking energy, E_b

Abrasive or particulate wear is observed for HNBR at

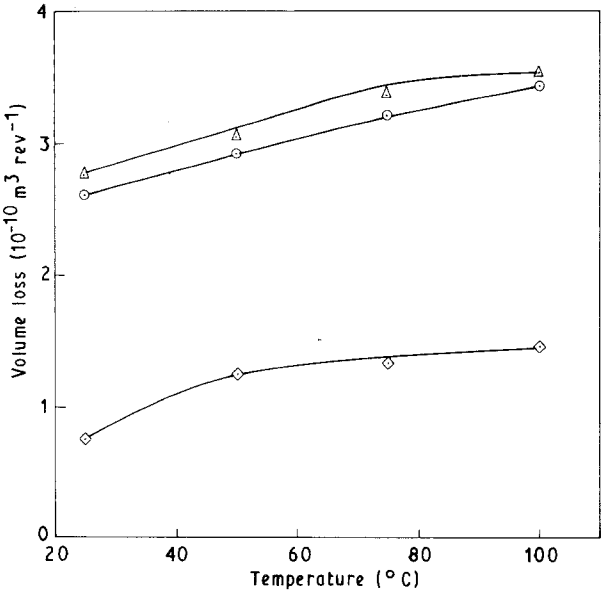

Figure 9 Variation of abrasion loss with temperature for NR, SBR and HNBR at 50 p.h.r. carbon black loading. (○) H4, (△) H8, (◇) D4.

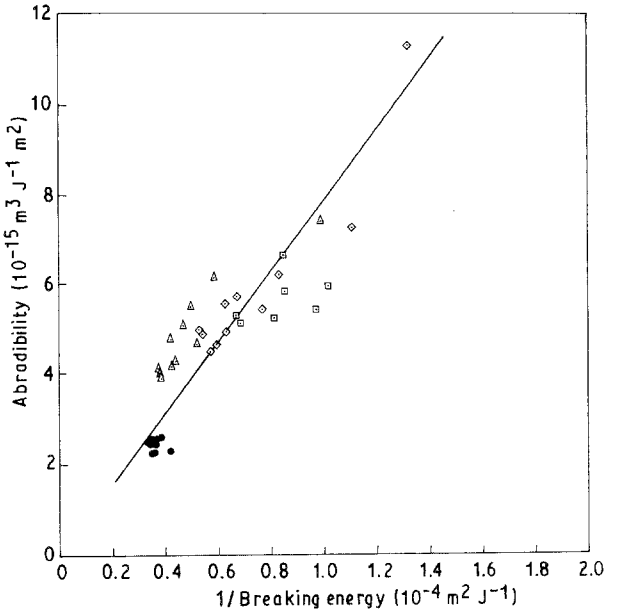

Figure 10 Relation between abradability and reciprocal of breaking energy (correlation coefficient = 0.85). (●) 25°C, (△) 50°C, (◇) 75°C, (□) 100°C.

all temperatures of abrasion. The abrasive wear process consists of the rupture of small particles of rubber under the action of frictional forces when sliding takes place between the rubber and the rough abrader surfaces. Hence it is expected that there may be a relation between the volume of material lost per unit frictional energy input, i.e. abradability, A, and the breaking energy, E_b. Grosch and Schallamach found a general parallel between A and the reciprocal of E_b [20], i.e.

$$A = C/E_b \tag{10}$$

The coefficient C represents the volume loss per unit frictional work done on a material for which the breaking energy is unity. A similar plot of A versus $(1/E_b)$ for filled compounds tested at various temperatures shows a linear relation (Fig. 10). The data points for gum compound are not in accord with Fig. 10. The value of C (from Fig. 10) is 5–12 $\times 10^{-12}$ m^3, which is the same as reported by Grosch and Schallamach [20].

3.6. Studies of abraded surface

The abraded surface of the HNBR compounds tested at 25°C does not show any ridges. However, some ploughing marks are observed in the direction of abrasion (Fig. 11). Similar results were reported for abrasion of HNBR against various rocks [10] and also with HNBR tank track pads against paved road [9]. However, the same compounds, above 50°C, show ridges perpendicular to the direction of abrasion. Schallamach [1] reported ridge formation in natural rubber (NR) compounds and suggested that the saw teeth bent back, leaving their underside exposed to abrasion and protecting a part of their rearside until they were torn off. Bhowmick [21] discussed the mechanism of ridge formation in NR compounds. The spacing between adjacent ridges is measured from the photographs taken at higher magnification and reported in Tables V and VI. The ridge spacing at any particular temperature decreases with loading of carbon black (Figs 12, 13) and resin (Figs 14, 15). The ridge spacing, however, increases with temperature (Table V).

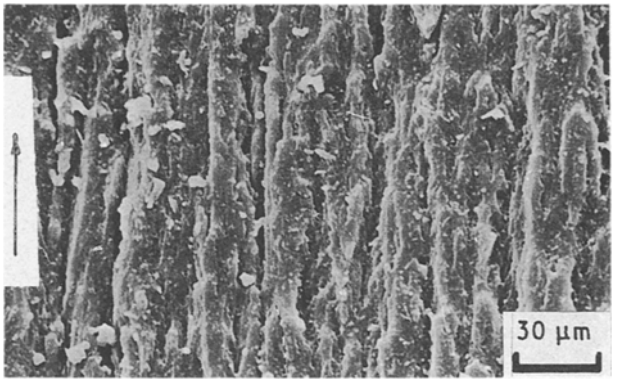

Figure 11 Scanning electron micrograph of abraded surface of compound D10 at 25°C.

TABLE V Ridge spacings at 100°C

Compound	Ridge spacing[a] (μm)
D5	37 ± 7
D6	26 ± 5
D7	21 ± 5
D8	27 ± 4
D9	93 ± 11
D10	73 ± 9
D11	53 ± 5
D12	43 ± 7
D13	30 ± 5
D2	22 ± 4

[a]Based on ten measurements on magnified photographs.

In order to understand the change in the mechanism of abrasion with temperature, G' and $\tan\delta$ at

TABLE VI Ridge spacing at different temperatures for D10

Temperature (°C)	Ridge spacings (μm)
25	No ridge
50	49 ± 7
75	62 ± 7
100	73 ± 9

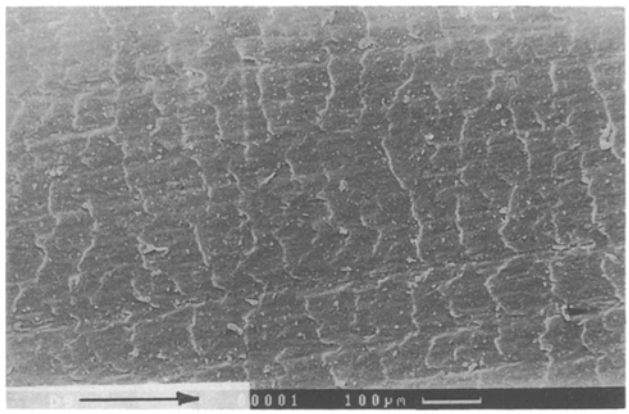

Figure 12 Scanning electron micrograph of abraded surface of compound D9 at 100°C.

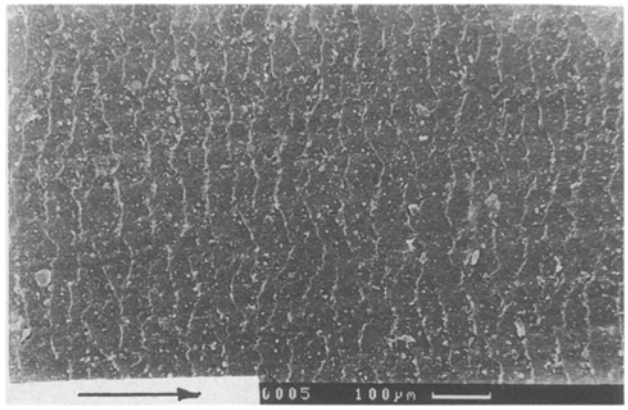

Figure 13 Scanning electron micrograph of abraded surface of compound D11 at 100°C.

10 Hz were measured from − 50 to + 150°C and the values extrapolated to the rate of deformation imposed by the asperities using WLF transformation. It is observed that the surface becomes leathery at 25°C at a high estimated rate of 1.5×10^4 Hz and, hence, there is no ridge formation. In this region, the change in tan δ with carbon black and resin loading is less [15] and hence μ and F for all the compounds at 25°C are close to each other. However, above 50°C, the surface at the rate of deformation imposed by the asperities, becomes rubbery and hence ridge formation takes place. Grosch and Schallamach reported a similar change in the abrasion mechanism with temperature for butyl rubber [6].

Schallamach related ridge spacing, R_s, with Hooke's modulus and normal load, P, by the following equation [22]

$$\text{ridge spacing, } R_s = \text{const.} \left(\frac{\phi}{E}\right) d \left(\frac{P}{E}\right)^{5/9} \quad (11)$$

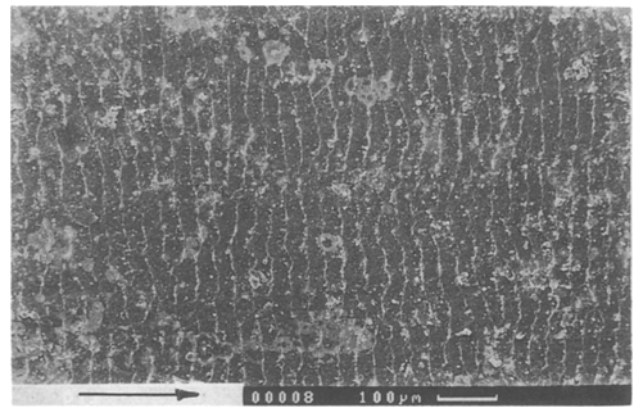

Figure 14 Scanning electron micrograph of abraded surface of control compound D12 (without resin) at 100°C.

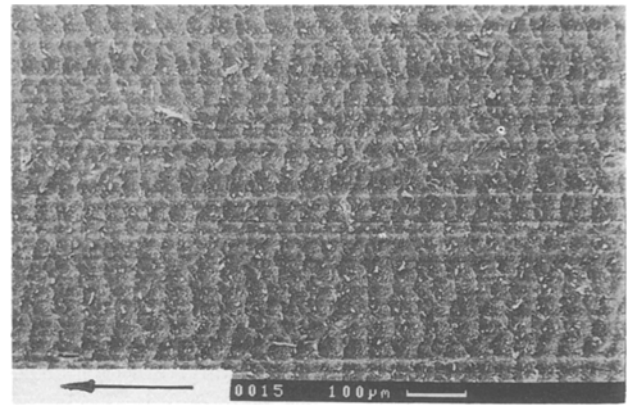

Figure 15 Scanning electron micrograph of abraded surface of compound D6 (20 p.h.r. resin) at 100°C.

where, $\phi = F/A$, F is the frictional force, and A the true area of contact and d the diameter of the abrasive grain.

In the present work, because the abrasion is carried out at constant normal load using same abrader, ϕ, P and d could be considered as constants. Hence Equation 11 could be rewritten as

$$R_s = \text{const.} \left(\frac{1}{E}\right)^{1.56} \quad (12)$$

During abrasion, the rubber surface is subjected to shearing and hence E may be replaced by the shear modulus G'

$$R_s = \text{const.} \left(\frac{1}{G'}\right)^{1.56} \quad (13)$$

The logarithmic plot of ridge spacing versus G' for different HNBR compounds tested at different temperatures gives a straight line with a slope of 1.55, as shown in Fig. 16. Considering the assumption in Equation 13, the fit is very good.

The abrasion loss is also plotted against ridge spacing (Fig. 17). The straight line intercepts the Y axis which indicates that abrasion takes place even in the absence of ridge formation. It is found that the abrasion loss increases with ridge spacing for compounds containing filler and resin. The relation between abrasion loss and ridge spacing could be explained by the fact that the compound is more

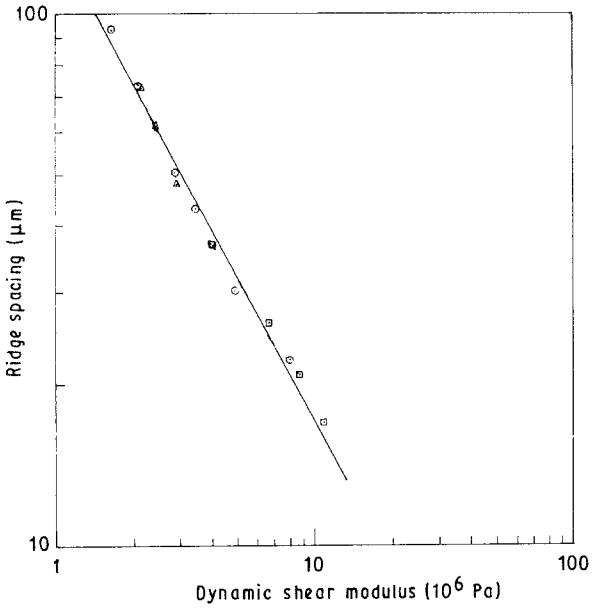

Figure 16 Relation between ridge spacing, R_s, and dynamic shear storage modulus, G'. (o) R_s (D9–D13, D2) at 100°C; (△) R_s (D10) at 50, 75, 100°C; (□) R_s (D5–D8) at 100°C.

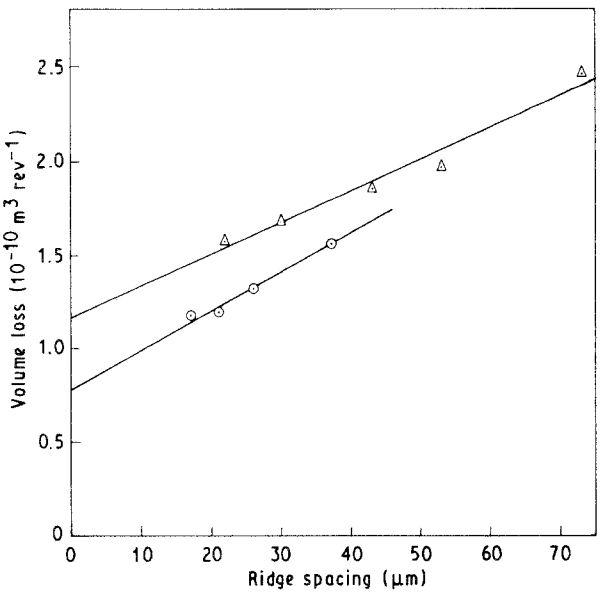

Figure 17 Relation between abrasion loss, V, and ridge spacing, R_s. (o) D5–D8 at 100°C, (△) D10–D13, D2 at 100°C.

susceptible to ridge formation at lower filler and resin loading and also at higher temperature. Once the ridge is formed, it accelerates the rate of wear [23] and grows with time of abrasion. Hence, the abrasion loss increases with ridge spacing.

4. Conclusions

1. The abrasion loss increases with decrease in cross-link density. Both sulphur- and peroxide-cured systems have similar abrasion loss at equal cross-link levels. The dynamic coefficient of friction, μ, and frictional force, F, decrease with cross-link density and temperature.

2. Incorporation of resin decreases the abrasion loss at all temperatures. μ and F decrease with resin loading and temperature.

3. The addition of carbon black decreases the abrasion loss and increases μ and F.

4. The abradability, A, increases linearly with reciprocal of breaking energy, $1/E_b$.

5. The abraded surfaces of all the compounds at 25°C do not show any ridges except ploughing marks along the direction of abrasion. Ridges are observed above 50°C. The ridge spacing decreases with carbon black as well as resin loading and increases with temperature. The ridge spacing, R_s, decreases linearly with dynamic shear storage modulus, G'. The abrasion loss, V, increases with ridge spacing, R_s.

References

1. A. SCHALLAMACH, in "Chemistry and Physics of Rubber Like Substances", edited by L. Bateman (MacLaren, London, 1963) Ch. 13, p. 382.
2. D. H. CHAMP, E. SOUTHERN and A. G. THOMAS, American Chemical Society, Coatings, Plastics Division, Paper 34 (1) (1974) p. 237.
3. A. N. GENT and C. T. R. PULFORD, *J. Appl. Polym. Sci.* **28** (1983) 943.
4. C. T. R. PULFORD, *Rubber Chem. Technol.* **58** (1985) 653.
5. K. A. GROSCH, *Proc. Roy. Soc. Lond. Ser. A.* **274** (1963) 21.
6. K. A. GROSCH and A. SCHALLAMACH, *Transactions* **41** (1965) T80.
7. C. W. EXTRAND, A. N. GENT and S. Y. KAANG, *Rubber Chem. Technol.* **64** (1) (1991) 108.
8. K. HASHIMOTO and Y. TODANI, in "Handbook of Elastomers", edited by A. K. Bhowmick and H. L. Stephens (Marcel Dekker, New York, 1988) Ch. 24, p. 741.
9. A. I. MEDALIA, A. I. ALESI, J. L. MEAD and R. SIMONAEU, Paper 34, presented at ACS meeting, Cincinnati, OH, October 1988.
10. P. THAVAMANI and ANIL K. BHOWMICK, *Rubber Chem. Technol.* **65** (1992) 31.
11. M. L. WILLIAMS, R. F. LANDEL and J. D. FERRY, *J. Amer. Chem. Soc.* **77** (1955) 3701.
12. B. ELLIS and G. N. WELDING, "Technique of Polymer Science" (Society of Chemical Industry, London, (1964) p. 46; *Rubber Chem. Technol.* **37** (1964) 571.
13. E. SOUTHERN, in "Elastomers: Criteria for Engineering Design", edited by C. Herpburn and R. J. W. Reynolds (Applied Science, London, 1979) Ch. 16, p. 273.
14. D. F. MOORE (ed.) "The Friction of Pneumatic Tyres" (Elsevier Scientific, New York, 1975) Ch. 1, p. 4.
15. P. THAVAMANI and ANIL K. BHOWMICK, *J. Mater. Sci.* **27** (1992) 3243.
16. A. R. PAYNE and R. E. WHITTAKER, *Rubber Chem. Technol.* **44** (1971) 440.
17. A. A. STAKLIS, *ibid.* **45** (1972) 1241.
18. C. NEOGI, S. P. BASU and A. K. BHOWMICK, *Plast. Rubber Process. Appl.* **12** (1989) 147.
19. A. K. BHOWMICK, C. NEOGI and S. P. BASU, *J. Appl. Polym. Sci.* **41** (1990) 917.
20. K. A. GROSCH and A. SCHALLAMACH, *Trans. Inst. Rubber Ind.* **41** (1965) 80.
21. A. K. BHOWMICK, *Rubber Chem. Technol.* **55** (1982) 1055.
22. A. SCHALLAMACH, *Wear* **1** (1958) 384.
23. *Idem, J. Appl. Polym Sci.* **12** (1968) 281.

Received 4 March
and accepted 30 June 1992